3.5 Phosphate stabilisation of partly oxidised, polymineralllic mine waste using solid and liquid phosphate fertilisers (experiment 3)

3.5.1 Aims

Experiment 2 demonstrated the ability of the phosphate stabilisation technique to form oxidation inhibiting, metal attenuating phosphate phases in partly oxidised, polymineralllic mine waste using liquid phosphate stabilisers. The chemical-grade KH_2PO_4 used in experiments 1 and 2 costs roughly A$50/kg, which prevents its use in large-scale remediation or mining operations. Phosphate fertilisers used in the agricultural industry are inexpensive enough to be used in large quantities (A$0.5 – A$2/kg). Soluble (liquid) and slightly soluble (solid) commercially-available phosphate fertilisers were used as a phosphate source in experiment 3 to determine whether these chemicals could be substituted for KH_2PO_4 in the phosphate stabilisation technique.

The specific aims of experiment 3 were:

a) to determine the morphologies and chemistries of any phosphate phases formed by the interaction of partly oxidised, polymineralllic mine waste with liquid and solid phosphate fertilisers;
b) to determine the stability, metal attenuation ability and acid generation inhibition ability of any phosphate phases formed by the interaction of partly oxidised, polymineralllic mine waste with liquid and solid phosphate fertilisers.

3.5.2 Specific methodology

The waste material and individual column set-up used in experiment 3 was identical to that used in experiment 2. The coating solutions, however, contained two commercial grade phosphate fertilisers as a phosphate source (Table 3.8). MKP is a phosphate fertiliser comprised of KH_2PO_4 but with higher levels of impurities than the chemical-grade KH_2PO_4 used in experiments 1 and 2. Trifos is a granular, partly soluble (solubility 18 g/l) solid fertiliser comprised

mostly of $Ca(H_2PO_4)_2$ with subordinate $CaNH_4HP_2O_7$ and $Ca(HPO_3H)_2$ (XRD results detailed in Appendix B9). The MKP was applied as a liquid, prepared by dissolving 109.66 g of the solid fertiliser in 2000 ml of distilled water, to which the other components of the coating solution were added. The Trifos was added as a solid on the top of the column, replacing the top layer of quartz sand in columns E, F and G. Samples of both fertilisers were subjected to a dissolution experiment (methodology and results presented in Appendix B9) in order to determine the exact chemistry of any impurities released into solution by the dissolution of the fertilisers. Significant quantities of As, Sb (MKP), Mn and Zn (Trifos) were released into solution by dissolution of the fertilisers. However, the absolute quantities of contaminants contributed to each leachate sample were not expected to be significant when compared with the input from the waste material.

Table 3.8. Coating solutions used in the coating stage of experiment 3.

	Oxidant	Phosphate	Buffer
Column A	0.2 M $KMnO_4$	0.4 M MKP	0.2 M CH_3COONa
Column B	0.1 M $KMnO_4$	0.4 M MKP	0.2 M CH_3COONa
Column C	-	0.4 M MKP	0.2 M CH_3COONa
Column E	0.2 M $KMnO_4$	100 g Trifos	0.2 M CH_3COONa
Column F	0.1 M $KMnO_4$	200 g Trifos	0.2 M CH_3COONa
Column G	-	200 g Trifos	0.2 M CH_3COONa

Potassium permanganate ($KMnO_4$) replaced H_2O_2 as an oxidant as it was considered more practical for use in field applications as it is easier and safer to handle. The coating solutions used in Columns C and G contained no $KMnO_4$ in order to determine whether an oxidant was necessary to form phosphate phases.

Five litres of coating solution were added to the columns at a rate of 400 ml per day. During the coating stage, leachate samples were collected after the addition of 200 ml, 2600 ml and 5000 ml of coating solution. These samples were analysed for As (2.5 mg/l), Cu (0.5 mg/l), Fe (0.5 mg/l), Pb (3 mg/l), S (4

mg/l), Sb (4 mg/l) and Zn (0.5 mg/l) by ICP-AES. Column E, F and G leachates were also analysed for P (1 mg/l) by ICP-AES. Detection limits are shown in brackets.

Prior to the commencement of the dissolution stage, as much of the remnant Trifos as possible was removed from the top of columns E, F and G. Due to partial dissolution and physical dispersion into the columns a small quantity (<10 g) of Trifos remained in columns E, F and G. The dissolution stage comprised the addition of 5000 ml of 0.01 M H_2O_2 at a rate of 400 ml per day. Leachate samples were collected after the addition of 200 ml, 800 ml, 1600 ml, 2000 ml and then every 600 ml addition until the addition of 5000 ml of oxidant. These samples were analysed for As (1 µg/l), Cu (0.1 µg/l), Pb (0.05 µg/l), Sb (0.1 µg/l) and Zn (5 µg/l) by ICP–MS and for Fe (0.1 mg/l), P (1 mg/l) and S (1 mg/l) by ICP-AES. Detection limits are shown in brackets. The results from the control column of experiment 2 were also used as a control for experiment 3 as the waste material and conditions (temperature and humidity) of both experiments were identical.

3.5.3 Coating stage results

Leachate chemistry

Complete chemical results for the coating stage leachates are tabulated in Appendix B4. The leachates of columns A, B and C remained between pH 5–6 throughout the coating stage of the experiment (Fig. 3.14a). In contrast, the leachate pH of columns E, F and G dropped for the first 1000–1400 ml coating solution addition and then climbed steadily for the remainder of the coating stage. Several jumps in the leachate pH occurred during the coating stage, which reference measurements of buffer solutions proved were caused by instrumental error. Degradation of the porous pin through contact with the $KMnO_4$ in the coating solutions was believed to have been the cause of the problem, therefore the electrode was replaced at the conclusion of the coating stage. Instrumental error caused a pH drift of approximately 0.6 units, therefore pH drift for columns A, B and C was limited to approximately 0.4 units. Even

accounting for the instrumental error, pH drift in the coating stage leachates of columns E, F and G was still >1 pH unit (Fig. 3.14a).

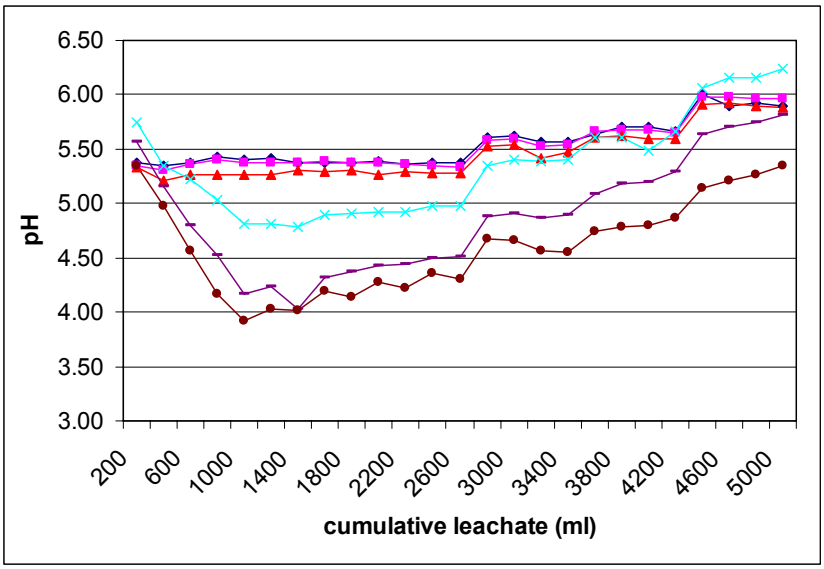

Figure 3.14a.

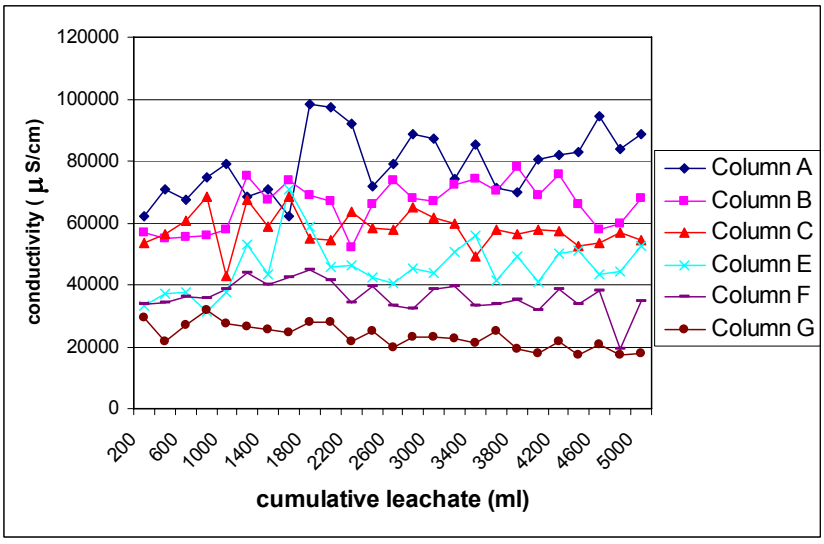

Figure 3.14b.

Figure 3.14. Experiment 3 pH (a) and conductivity (b) of coating stage leachates. Legend for (b) also applies to (a).

The conductivities of the coating stage leachates were very high (17 000 µS/cm – 98 000 µS/cm) and varied greatly between columns (Fig. 3.14b). The relative column leachate conductivities (column A > column B > column C > column E >

column F > column G) can be related to the concentrations of the phosphate and oxidant used in the coating solutions (Table 3.8).

The trace element detection levels for the coating stage leachates were relatively high (Section 3.5.2). This was due to the application of high dilution factors necessitated by the use of $KMnO_4$ in most coating solutions, which would otherwise have interfered with the spectrometer (Hu, Y. pers. comm. 2002). Iron, Pb and Sb were below detection in all leachates. With the exception of P, elemental concentrations decreased during the coating stage (Fig. 3.15). Arsenic and Zn values were below detection levels for most of the coating stage. Copper was only detected in column C, E and G leachates. Phosphorous concentrations, analysed only in column E, F and G leachates to give an indication of the extent of Trifos dissolution, were highest in the middle of the coating stage (Fig. 3.15b). The relative elemental abundance for those elements detected was SO_4^{2-} > Cu > Zn > As, which was similar to the order of the most abundant elements in the coating stage leachates of experiments 1 and 2.

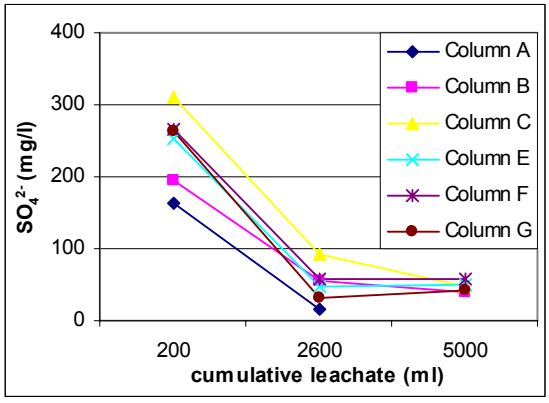

Figure 3.15a. SO_4^{2-}

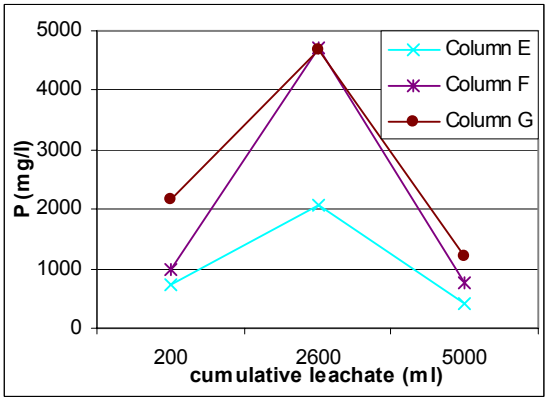

Figure 3.15b. P

Figure 3.15. Concentrations of SO_4^{2-} (a) and P (b) in coating stage leachates of experiment 3.

SEM observations

A summary of the post-coating stage SEM observations is presented in Table 3.9. Detailed results and additional SEM micrographs are presented in Appendix B7. Generally the extent of phosphate phase formation was greater in experiment 3 than in experiments 1 and 2. The relative abundance of phosphate formation in the coated columns was: column E > column F > column A > column B > column G > column C. However, this does not apply to all specific phosphate phases. Pb and Fe phosphate phases were most abundant in column C. Many of the phosphate phases formed in experiment 3 displayed very different morphologies and chemistries to those observed in the previous two experiments. This was most likely due to the difference in coating solutions. Columns A, B, E and F contained abundant Mn phosphate phases (Fig. 3.16a,e) ($KMnO_4$ as oxidant), whereas in column G, Ca phosphates were most abundant (Fig. 3.16c) ($Ca(H_2PO_4)_2$ as phosphate source, no $KMnO_4$). Rosettes of Cu+K-Ca phosphate were the only discrete metal phosphate phase abundant in all columns (Fig. 3.16e). Lead phosphates were only abundant in column C material (Fig. 3.16f). Zinc phosphates were not observed in any column. Significant quantities of metals tended to be incorporated into the Mn or Ca phosphates (Fig. 3.16a,d) (representative EDS trace in Appendix B8), except in column C which lacked abundant quantities of either of these phases.

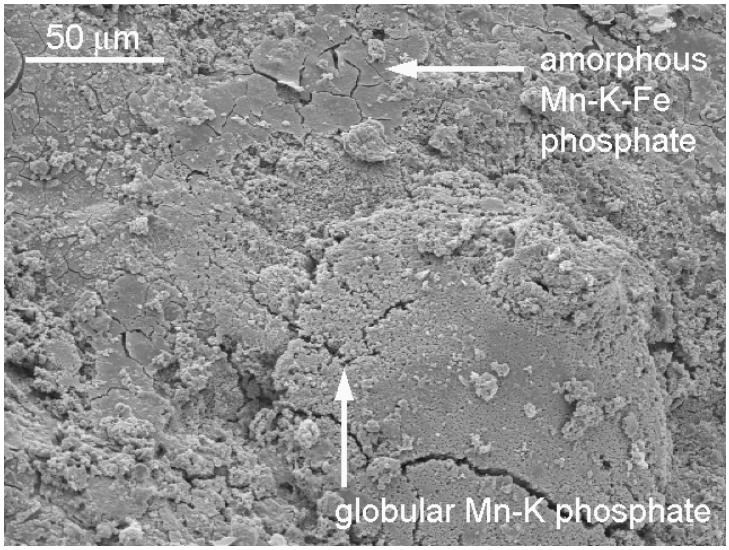

Figure 3.16a.

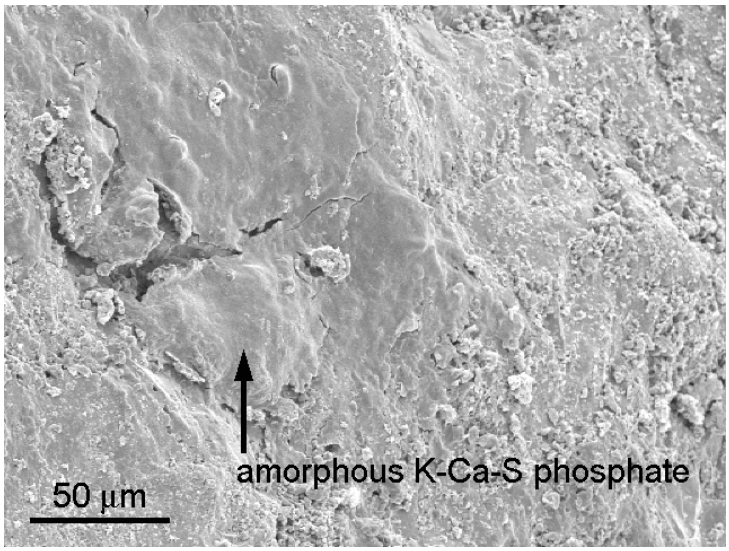

Figure 3.16b.

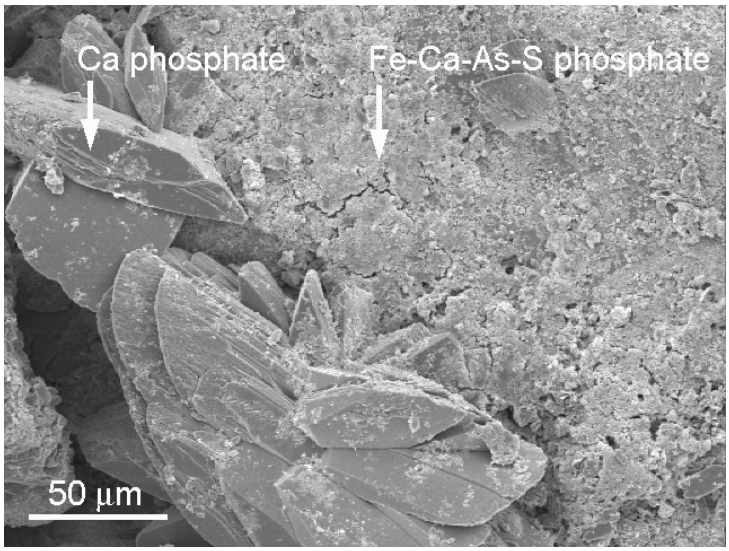

Figure 3.16c.

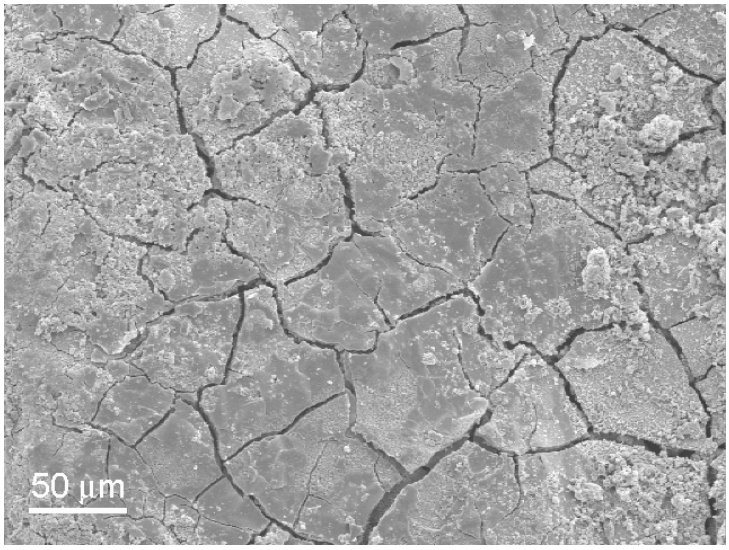

Figure 3.16d.

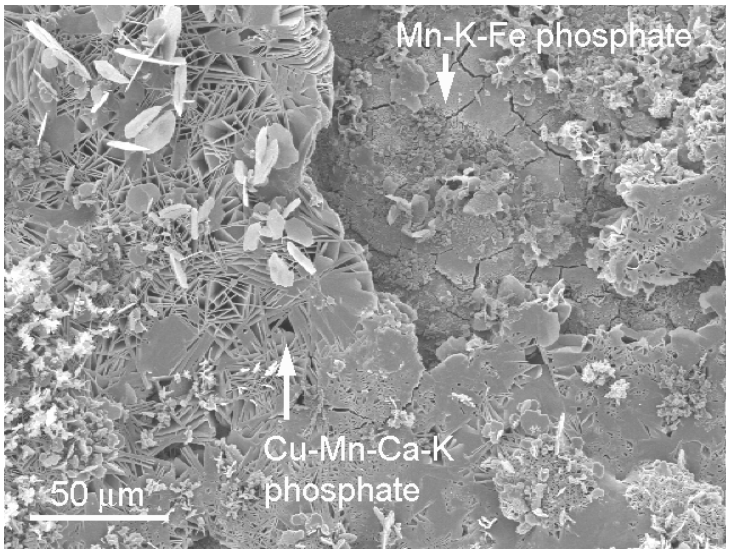

Figure 3.16e.

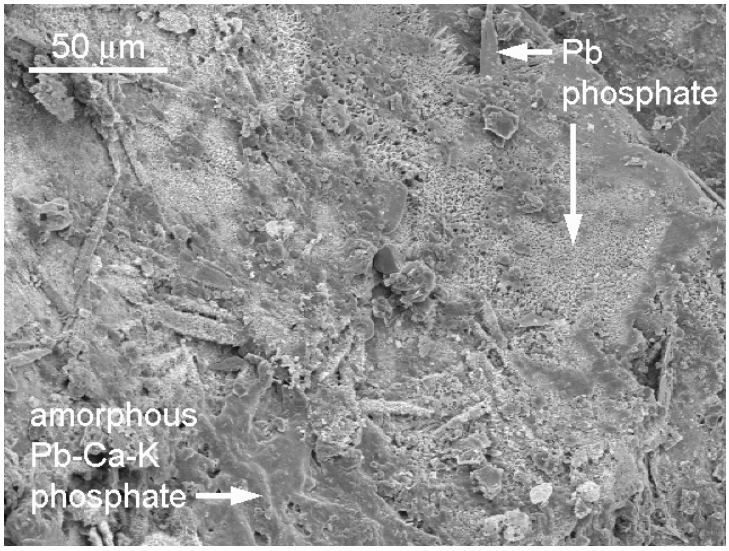

Figure 3.16f.

Figure 3.16. SEM micrographs of material removed from the coated columns after the coating stage of experiment 3. a) Globular Mn-K phosphate covering amorphous Mn-K-Fe phosphate coating, column B. b) Amorphous K-Ca-S phosphate coat on tetrahedrite, column B. c) Granular Fe-Ca-As-S phosphate precipitates on chalcopyrite and large Ca phosphate crystals, column G, EDS trace of similar material in Appendix B8. d) Amorphous Mn-Ca-Pb-Zn phosphate coating on sphalerite, column E. e) Mn-K-Fe phosphate coating on chalcopyrite with adjacent Cu-Mn-Ca-K phosphate rosettes covering Cu sulphates, column B. f) Acicular crystals and pincushions of Pb phosphate and amorphous Pb-Ca-K phosphate coating on galena, column C.

The abundant Mn and Ca phosphates usually formed multiple layers on sulphides. An amorphous coating was often covered by granular precipitates relatively rich in Mn or Ca (Fig. 3.16a). Chalcopyrite was again the most effectively coated sulphide, although the granular Mn and Ca phosphates were observed on all phases including tetrahedrite (Fig. 3.16b) and quartz.

Indurations of mineral grains, cemented together by granular Mn phosphate and Ca phosphate precipitates, were formed in columns E, F and G. These indurations were formed at the top of the waste material directly below the layer of solid Trifos and had thicknesses of 3cm in column E and 1 cm in columns F and G. Copper sulphate rosettes were observed in all columns and Ca/K sulphates in columns C and E. Other sulphate phases were only rarely observed and sulphate abundances overall were generally less in experiment 3 than in experiments 1 and 2.

3.5.4 Dissolution stage results

Leachate chemistry

Complete chemical results for the dissolution stage leachates are tabulated in Appendix B4. The pH of all coated column leachates remained above that of the control column leachate for the duration of the dissolution stage. There were distinct differences in the pH trends between the coated column leachates (Fig. 3.17a). Column A and B leachate pH values were initially 7.3, gradually declining for the first half of the dissolution stage before stabilising at pH 6.9. Column C leachate pH was also initially 7.3, however, the leachate pH decreased steadily throughout the dissolution stage, finishing with a value of 5.9. Column E leachate pH remained close to 6.9 for the duration of the dissolution stage. The leachate pH of Columns F and G both rose steadily at the start of the dissolution stage and stabilised at values of 6.9 and 6.2 respectively. Unlike columns A, B and C, and the coated columns of experiment 1 and 2, the leachate pH of columns E, F and G did not rise significantly upon the addition of $Ca(OH)_2$.

The conductivities of all coated column leachates decreased rapidly from an initial high, and then slowly until the conclusion of the dissolution stage (Fig. 3.17b). With the exception of column C leachates, conductivities were significantly higher than the control column values and the values of dissolution stage coated column leachates in experiments 1 and 2. The observation of extensive flushing of coating stage solutions and remobilisation of precipitates

Table 3.9. Summary of SEM observations of precipitates formed on partly oxidised, polymineralic mine waste in columns during the coating stage of experiment 3.

Chemistry	Morphology	Abundance
Mn-K±Ca, Cu, Fe, Pb, S, Zn, (As, Al, Si) phosphate (Fig. 3.16a,d,e)	generally thick (>3 µm) coatings of amorphous (Fe or Pb), flaky, globular, granular and fine-grained rosette (Cu) aggregates, usually with desiccation cracks; coatings often covered by granular or rosette precipitates; granular precipitates at top of column cemented together grains to form indurations in columns E and F	coating on ~99 % of chalcopyrite, galena and stannite, >50 % sphalerite in columns A, B, E and F, >50 % tetrahedrite in column A and B; pyrite and arsenopyrite uncoated, precipitates on all phases including quartz and clays
Cu±K, Ca, Mn, (S, Fe, Cl) phosphate (Fig. 3.16e)	spherical rosettes and botryoids up to 100 µm diameter, often form coalescences of radial splays; amorphous coating with desiccation cracks; granular precipitates	rosettes heterogeneous, cover 100 % of some grains, preferentially associated with well-coated grains in all columns; botryoids only in column G; amorphous coatings rare in columns A, B
Pb±Ca, K, (Zn) phosphate (Fig. 3.16f)	amorphous coatings; fine-grained (0.5 µm x 5 µm) coalescences of acicular pincushions; granular precipitates; rosettes; euhedral booklets; large (100 µm x 30 µm) tabular and bi-pyramidal crystals; acicular radial splays	pincushions cover ~75 % of galena surfaces in column C, ~5 % in column B; other phases common precipitates on coated galena in column C, scattered precipitates in columns A, B and E; amorphous coatings only in column C
Fe-K-Cu phosphate	amorphous coating with desiccation cracks, usually covered by granular Mn phosphate in column A	thin coating on <50 % of chalcopyrite in column C, rare coating in column A

Table 3.9 continued.

Chemistry	Morphology	Abundance
Ca±K, Cu, Fe, Al, S, Pb, Cl, (As, Zn) phosphate (Fig. 3.16b,c)	granular and globular precipitates; amorphous coats with desiccation cracks; large (100 µm x 50 µm) euhedral prisms and radial splays; granular precipitates at top of column G cemented together grains to form indurations	cover >80 % of chalcopyrite, 50 % of galena, arsenopyrite, 40 % tetrahedrite in column G; scattered precipitates and coats on all phases in columns B, C, E and F; prisms and splays often associated with relict Trifos granules in columns E and F
Cu, Ca, K-Ca, Pb-Al-Cu, Fe-Zn-Cu sulphates	hexagonal rosettes (10 µm diameter); fibres; dendrites and prismatic crystals	Cu sulphate rosettes associated with coalescences of Cu phosphate rosettes cover up to 10 % of grains in all columns; other phases scattered precipitates in columns B, C and E

into the leachates at the start of the dissolution stage explains the high conductivities.

The general metal and metalloid leachate chemistry trends identified in experiment 3 are the same as in experiments 1 and 2. Base metal concentrations in the coated column leachates were much lower than the control column leachate values, generally by an order of magnitude (Fig. 3.18c,e,f). The metalloid concentrations in the coated column leachates were higher than in the control column leachates (Fig. 3.18a,g). However, there was considerable variation in leachate trends between elements and between columns for some individual elements.

The $[SO_4^{2-}]$ in the dissolution stage leachates of all columns except column G was initially relatively high and decreased rapidly before stabilising below 20 mg/l (Fig. 3.18b). Iron concentrations were generally below detection (0.1 mg/l) in all columns except columns C and G. Column C leachate [Fe] was below 1 mg/l throughout the dissolution stage whilst column G leachate [Fe] fell rapidly

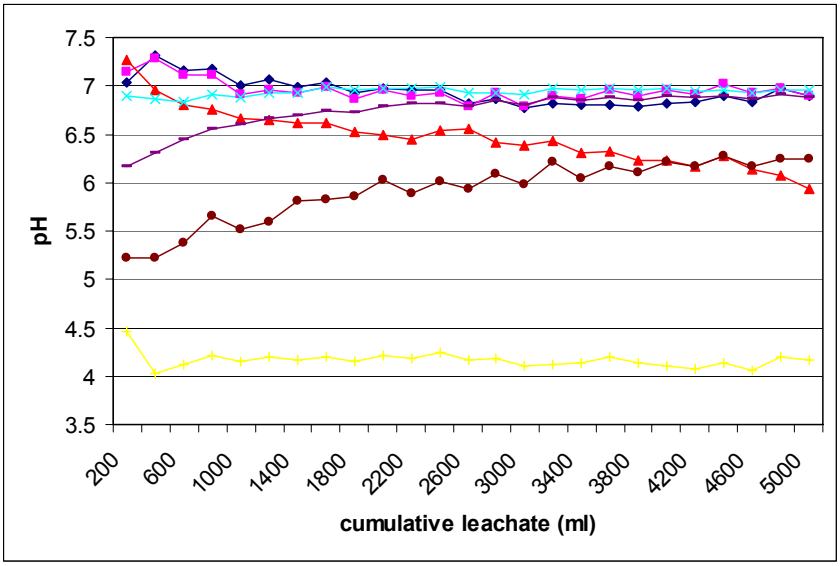

Figure 3.17a.

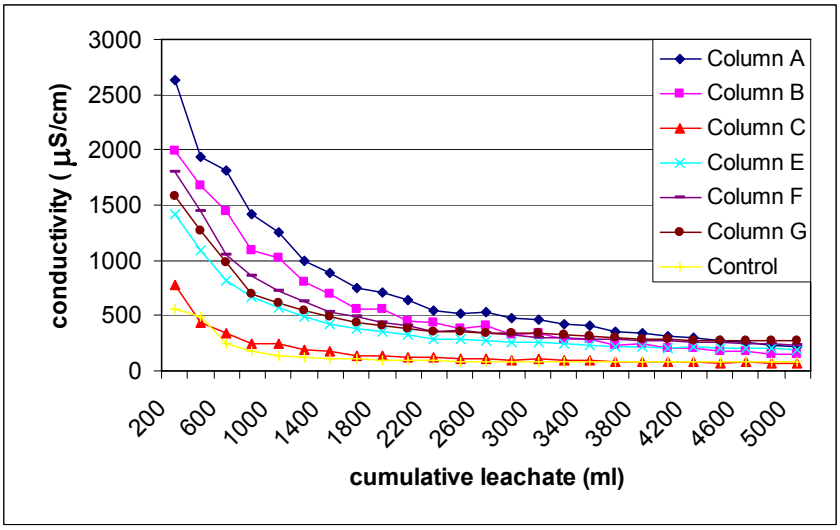

Figure 3.17b.

Figure 3.17. Experiment 3 pH (a) and conductivity (b) of dissolution stage leachates. Legend for (b) also applies to (a).

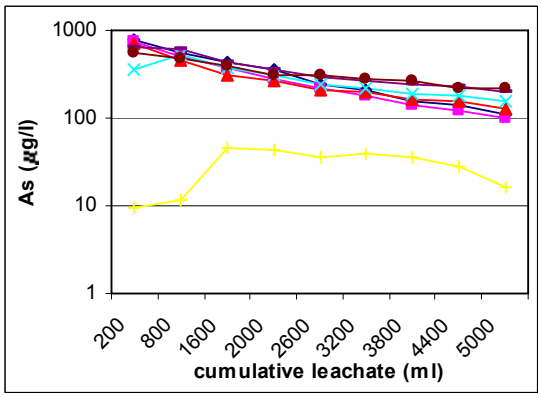

Figure 3.18a. As

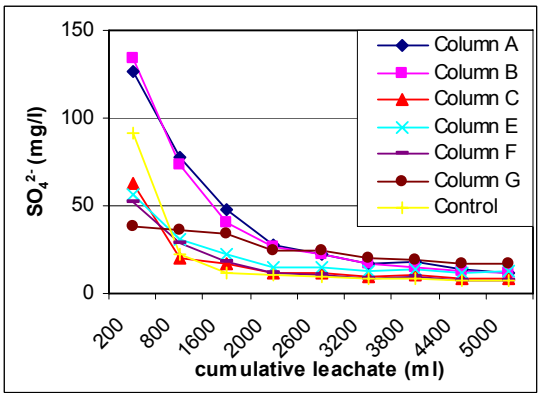

Figure 3.18b. SO_4^{2-}

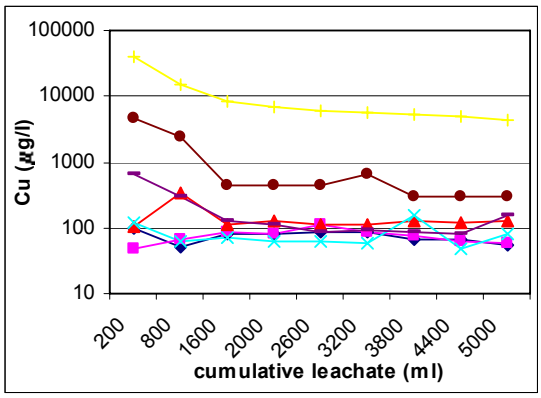

Figure 3.18c. Cu

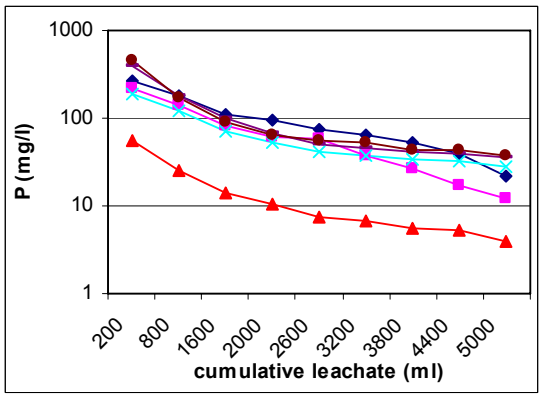

Figure 3.18d. P

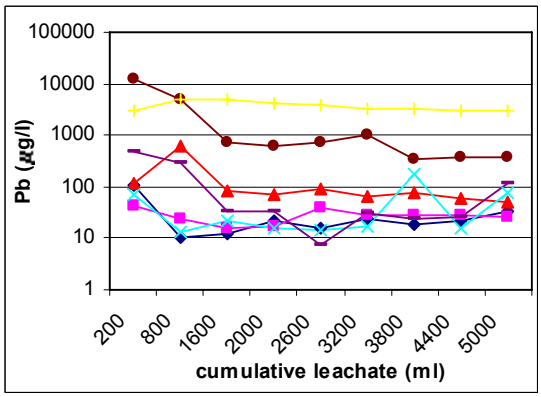

Figure 3.18e. Pb

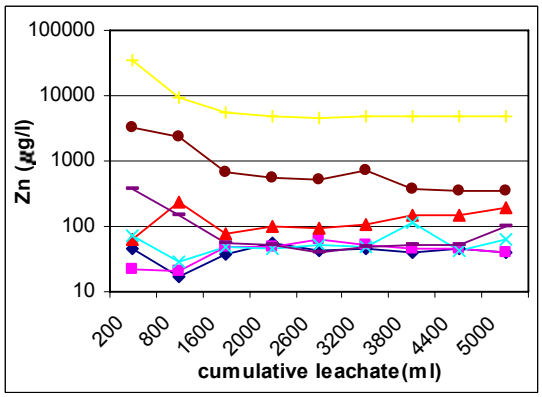

Figure 3.18f. Zn

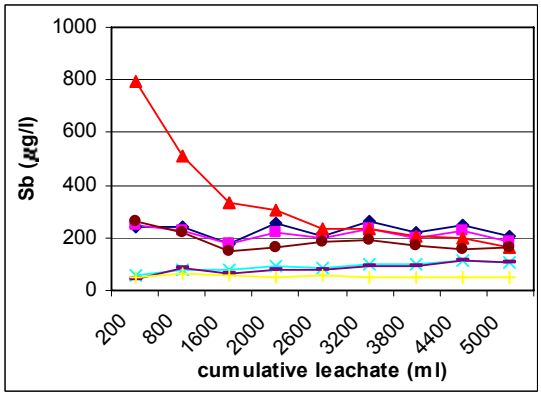

Figure 3.18g. Sb

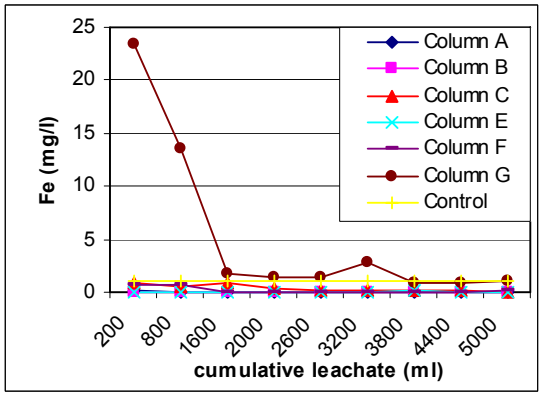

Figure 3.18h. Fe

Figure 3.18. Concentrations of elements in dissolution stage leachates of experiment 3. Legends for (b) and (h) are applicable to all graphs.

from 23 mg/l before stabilising (Fig. 3.18h). Leachate trends for the base metals were similar to each other, despite variations between the columns (Fig. 3.18c,e,f). The base metal concentrations in the Column G leachates were the highest of the coated columns throughout the dissolution stage, the levels of Pb initially being higher than in the control leachates. The base metal concentrations in the column F leachates also decreased rapidly from an initial

high before stabilising at values similar to the other coated column leachates. The base metal concentrations in the column A, B, C and E leachates remained relatively low throughout the dissolution stage. Copper and Zn leachate values did not increase during the dissolution stage, with the exception of column C [Zn] (Fig. 3.18f), which is in contrast to the previous two experiments. Arsenic concentrations decreased rapidly from an initial high in the leachates of all coated columns during the dissolution stage (Fig. 3.18a). Trends of [Sb], in contrast, were dissimilar to those in the previous experiments, with the exception of column C, in which the [Sb] decreased rapidly from an initial high (Fig. 3.18g). The Sb concentrations in the other coated column leachates remained relatively low throughout the dissolution stage. Column E and F leachate [Sb] showed a slight increase during the dissolution stage. The [P] in the coated column leachates showed a rapid decrease from an initial high and then a slow decrease for the remainder of the dissolution stage (Fig. 3.18d).

The relative elemental abundance in the coated column leachates during the dissolution stage of experiment 3 (cumulative element release throughout the dissolution stage), varied between the coated columns, which is in contrast to experiments 1 and 2. The relative elemental abundances were as follows:

Columns A, B and E:	SO_4^{2-} > As > Sb > Cu > Zn > Pb > Fe.
Column C:	SO_4^{2-} > Fe > Sb > As > Cu > Pb > Zn.
Column F:	SO_4^{2-} > As > Fe > Cu > Pb > Zn > Sb.
Column G:	SO_4^{2-} > Fe > Pb > Cu > Zn > As > Sb.

These differ significantly from the relative cumulative elemental abundance in the control column leachates, which was SO_4^{2-} > Cu > Zn > Pb > Al > Sb > As > Fe.

SEM observations

A summary of the SEM observations (on the waste material removed from the columns at the conclusion of the dissolution stage of the experiment) is presented in Table 3.10. Detailed results and additional SEM micrographs are

Table 3.10. Summary of SEM observations of precipitates and coatings found on partly oxidised, polymineralic mine waste after the conclusion of the dissolution stage of experiment 3.

Chemistry	Morphology	Abundance
Mn-K±Ca, Cu, Fe, Pb, S, Zn, (As, Al, Si) phosphate (Fig. 3.19a,c,d)	identical to the Mn phosphates observed after the coating stage except for the presence of scattered prisms and radial splays of crystals (Mn±Zn, Ca) in columns A and B; granular indurations persisted in columns E and F	flaky, granular and globular precipitates less abundant; amorphous coatings appear more abundant and observed heterogeneously on all sulphides including pyrite and arsenopyrite
Cu±K, Ca, Mn, (S, Fe, Cl) phosphate (Fig. 3.19a,d)	spherical rosettes up to 100 µm diameter, often form coalescences of radial splays which grade into granular agglomerates with significant Mn or Ca; rare evidence of corrosion	generally extensive where present (covers >50 % of grain), Cu sulphates form preferential substrate; scattered precipitates only present in columns E, F and G
Pb±Ca, K, (Zn) phosphate (Fig. 3.19b)	fine-grained (0.5 µm x 5 µm) acicular pincushions; tabular, prismatic and bean-shaped crystals; radial splays; globular agglomerates; botyroids	pincushions cover ~90 % of galena surfaces in column C, <1 % in columns B and E; other phases common precipitates on coated galena in column C, scattered precipitates in columns A, B
Fe-K-Cu±Ca phosphate	amorphous coating with desiccation cracks; granular and globular precipitates	only in column C, thin coating on ~25 % of chalcopyrite; precipitates scattered on chalcopyrite and tetrahedrite
Ca±K, Mn, Cu, Fe, Al, S, Pb, Cl, (As, Zn) phosphate	granular and globular precipitates; amorphous coats with desiccation cracks; large (200 µm x 50 µm) euhedral prisms and radial splays; induration in column G appeared degraded	compared with after the coating stage amorphous coatings in column G less abundant; granular precipitates less abundant in column C but more abundant in columns E and F

Table 3.10 continued.

Chemistry	Morphology	Abundance
Cu, Ca, K-Mn, Pb±Cu, Fe; Cu-Ca-Zn sulphates	rosettes (up to 50 μm diameter); botryoids; fibres; dendrites; radial splays; globular agglomerates; amorphous precipitates; prismatic crystals	Cu sulphate rosettes associated with Cu phosphate rosette coalescences, cover up to 10 % of grains in all columns; Ca phases abundant in columns E, F and G; Pb phases only common in column C; other phases rare precipitates in columns B and C

presented in Appendix B7. The overall order of extent of phosphate development after the dissolution stage was the same as after the coating stage (i.e. column E > column F > column A > column B > column G > column C). Amorphous coatings appeared more abundant in columns A, B and F after the dissolution stage (Fig. 3.19c). This is interpreted to be the result of granular precipitate removal, which revealed amorphous coatings on sulphide surfaces that were previously obscured by the granular precipitates. It is probable that the granular precipitates observed in column E were so extensive that an insignificant amount of amorphous coatings were exposed despite the removal of granular precipitates during the dissolution stage.

Abundances of Cu and Pb phosphate phases appeared unchanged after the dissolution stage. However, evidence of corrosion of Cu-Mn phosphate rosettes was occasionally observed in column A (Fig. 3.19a). Variations in phosphate morphology and chemistry, often in the form of additional incorporated Mn, Ca or Zn at the expense of K, were commonly observed. This was particularly evident in column C. Lead phosphates showed the most variation, including textures showing possible corrosion and re-precipitation in column C (Fig. 3.19b). Rare Zn phosphates were present in column C, which were not observed prior to the dissolution stage. Large crystals and granular precipitates of Ca phosphate were also more abundant after the dissolution stage in column E and F. The amount of sulphates observed in the columns after the dissolution

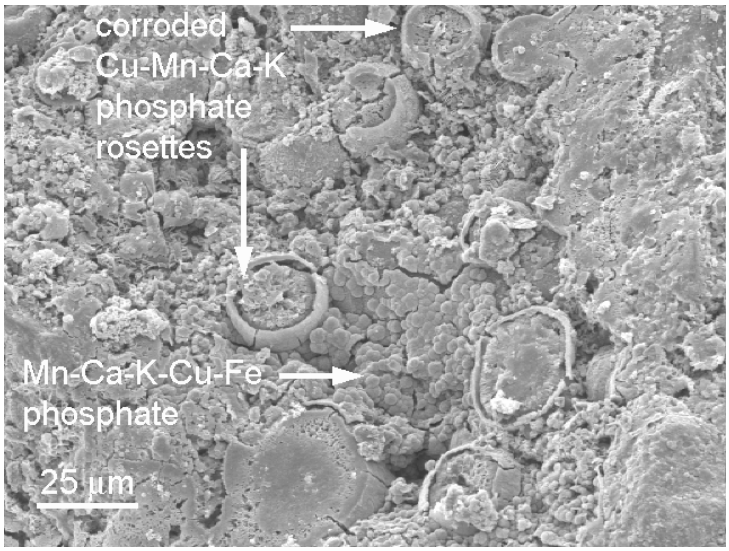

Figure 3.19a.

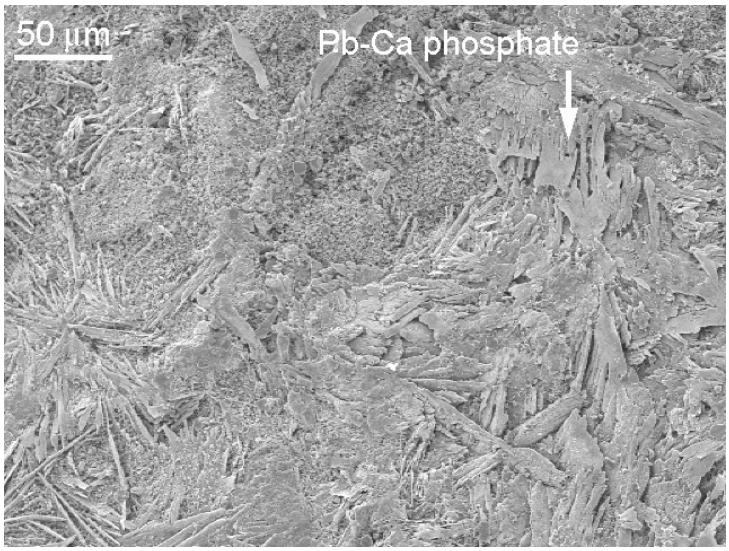

Figure 3.19b.

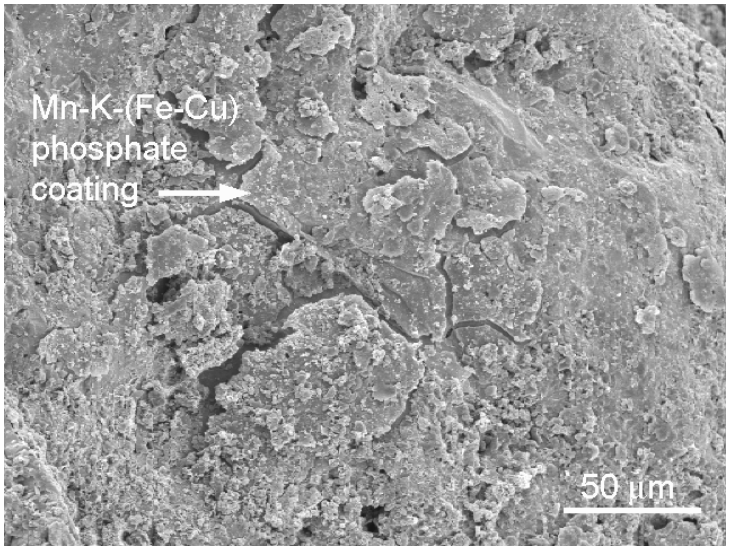

Figure 3.19c.

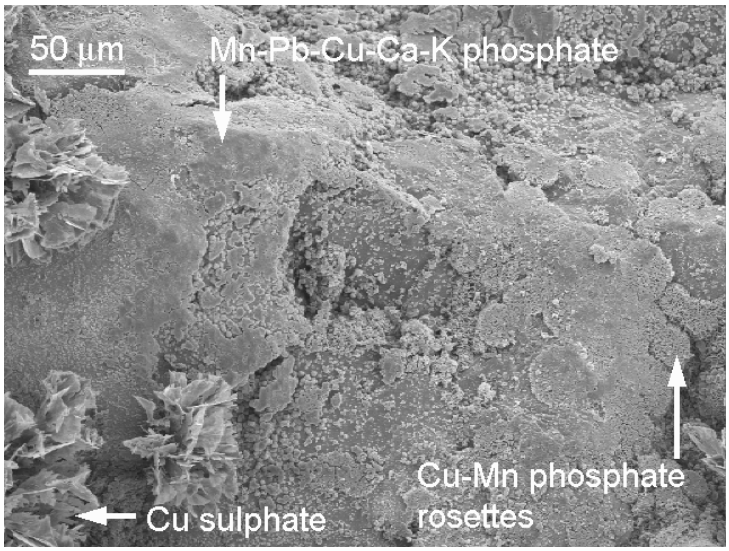

Figure 3.19d.

Figure 3.19. SEM micrographs of material removed from the coated columns after the dissolution stage of experiment 3. a) Cu-Mn-Ca-K phosphate rosettes showing evidence of corrosion precipitated on botryoidal Mn-Ca-K-Cu-Fe phosphate coating chalcopyrite, column A. b) Tabular Pb-Ca phosphate crystals with melted texture, possibly indicative of corrosion and re-precipitation, column C. c) Thin, poorly-developed Mn-K(Fe-Cu) phosphate coating on tetrahedrite, column A. d) Globular Mn-Pb-Cu-Ca-K phosphate coating on galena covered by Cu-Mn phosphate rosettes and Cu sulphate rosettes, column B.

stage were generally similar to those observed in the coated columns. However, the abundances of Cu and Pb sulphates in column C and Ca sulphates in columns E, F and G were greater after the dissolution stage.

3.5.5 Discussion

Formation of phosphate phases

The more extensive degree of phosphate formation observed in experiment 3 can be attributed to the coating solution chemistry. The use of $KMnO_4$ as an oxidant in the coating solutions of columns A, B, E and F supplied abundant Mn^{2+} and K^{+}, which reacted with the PO_4^{3-}. This resulted in extensive Mn-K phosphate development. In addition, the use of Trifos ($CaH_4(PO_4)_2$) in columns E, F and G released abundant Ca^{2+} into solution, resulting in Mn-K-Ca phosphate formation in columns E and F, and Ca phosphate formation in column G. The presence of an amorphous, often metal-rich coating on many

sulphides in columns A, B, E and F, covered in turn by granular precipitates relatively rich in Mn and Ca (Fig. 3.16a), indicates that two different phosphate forming processes occurred in these columns. Firstly, the $KMnO_4$ oxidised the sulphide surface, releasing metal cations which complexed with the phosphate anions and coated the sulphide surface. Possible reactions for this process involving chalcopyrite and galena (the most commonly coated sulphides) in columns A and B are:

$$CuFeS_{2(s)} + KMnO_{4(l)} + 2KH_2PO_{4(l)} + 2O_{2(aq)} \rightarrow (Mn,K,Fe)(PO_4)_{2(s)} + 2SO_4^{2-}{}_{(aq)} + Cu^{2+}{}_{(aq)} + 2K^{+}{}_{(aq)} + 4H^{+}{}_{(aq)} \quad (3.12)$$

$$3PbS_{(s)} + 3KMnO_{4(l)} + 5KH_2PO_{4(l)} \rightarrow (Mn,K,Pb)_3(PO_4)_{5(s)} + 3SO_4^{2-}{}_{(aq)} + 5K^{+}{}_{(aq)} + 10H^{+}{}_{(aq)} \quad (3.13)$$

In columns E and F, in which Trifos was used as a phosphate source, possible reactions are:

$$3CuFeS_{2(s)} + 3KMnO_{4(l)} + 4Ca(H_2PO_4)_{2(s)} + 6O_{2(aq)} \rightarrow (Mn,K,Ca,Fe)_3(PO_4)_{8(s)} + 6SO_4^{2-}{}_{(aq)} + 3Cu^{2+}{}_{(aq)} + Ca^{2+}{}_{(aq)} + 16H^{+}{}_{(aq)} \quad (3.14)$$

$$3PbS_{(s)} + 3KMnO_{4(l)} + 3.5Ca(H_2PO_4)_{2(s)} \rightarrow (Mn,K,Ca,Pb)_3(PO_4)_{7(s)} + 3SO_4^{2-}{}_{(aq)} + 0.5Ca^{2+}{}_{(aq)} + 14H^{+}{}_{(aq)} \quad (3.15)$$

The second phosphate forming process involved reaction of the cations disassociated from the oxidant directly with the phosphate anions:

$$KMnO_{4(l)} + KH_2PO_{4(l)} \rightarrow (Mn,K)PO_{4(s)} + K^{+}{}_{(aq)} + 2O_{2(aq)} + 2H^{+}{}_{(aq)} \quad (3.16)$$

$$KMnO_{4(l)} + 3Ca(H_2PO4)_{2(s)} \rightarrow (Mn,K,Ca)_3(PO4)_{5(s)} + PO_4^{3-}{}_{(aq)} + 6O_{2(aq)} + 12H^{+}{}_{(aq)} \quad (3.17)$$

The fact that these granular phases are precipitated indiscriminately on all phases in the columns, including chemically inert minerals such as quartz (Fig.

3.20), shows that no interaction with the substrate was required for their formation.

The high concentrations of Mn, K and/or Ca in columns A, B, E, F and G prevented the saturation of base metal phosphates developing within the columns, explaining their relative paucity. Instead the Cu^{2+}, Pb^{2+} and Zn^{2+} cations were readily incorporated into the Mn/Ca-rich coatings and precipitates. This also explains the below detection base metal concentrations in the leachates of the coated columns during the coating stage, except for Cu and Zn in columns C and G. Sulphate was also often incorporated into the granular precipitates, especially the Mn-rich phosphates of column A and B. This controlled the coating stage leachate [SO_4^{2-}], rather than sulphide oxidation, explaining the relatively high column C and low column A and B coating stage leachate [SO_4^{2-}] (Fig. 3.15a). This was despite the fact that the column C coating solution contained no oxidant other than H_2O. The lack of abundant Mn or Ca phosphates in column C allowed the development of Pb phosphates (Fig. 3.16f; Fig. 3.19b). Rosettes of Cu phosphate were observed in all columns, though only where Cu phosphate saturation was reached through the dissolution of Cu sulphates (Reaction 3.11).

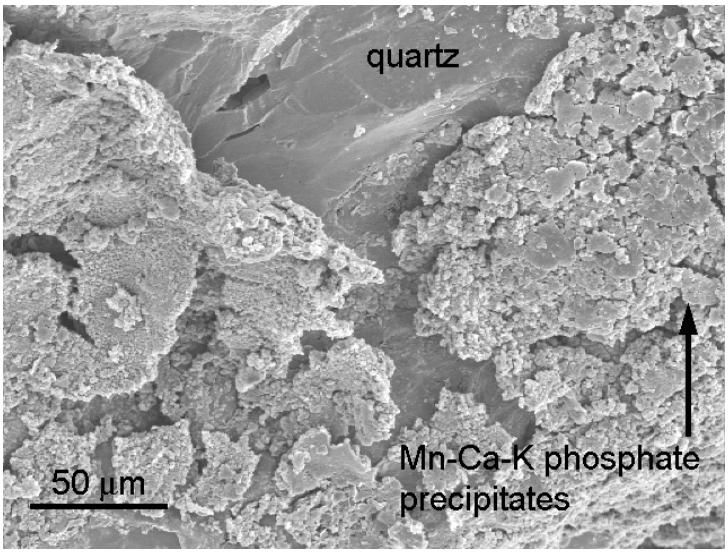

Figure 3.20. Granular Mn-Ca-K phosphate precipitates on quartz, column E, post-coating stage.

The column E, F and G coating stage leachates were not successfully buffered between pH 5-6 throughout the coating stage (Fig. 3.14a). The leachate trend indicated a rapid production of acidity for the first 1000–1400 ml of coating solution addition, followed by a gradual decrease in acid production until the end of the coating stage. The dissolution of MKP (KH_2PO_4, Reaction 3.1, Section 3.3.3) results in the production of half as much acid as the dissolution of Trifos:

$$Ca(H_2PO4)_{2(s)} \rightarrow Ca^{2+}{}_{(aq)} + 2PO_4{}^{3-}{}_{(aq)} + 4H^{+}{}_{(aq)} \quad (3.18)$$

This suggests that the pH in the column E, F and G leachates was controlled by the dissolution of Trifos during the coating stage. Differential dissolution kinetics of the Trifos may explain the pH trends of the coating stage leachates, whereby rapid initial dissolution of the readily soluble Trifos overcame the buffering capacity of the NaAC for the first ~1400 ml of coating solution addition (M. Liddell, pers. comm. 2003). Depletion of the readily soluble Trifos resulted in less acid generation, allowing the NaAC to buffer the leachate to higher pH values for the remainder of the coating stage. Immersion of 50 g of Trifos in 500 ml of distilled water resulted in an instantaneous pH drop from 5.9 to 3.3, demonstrating the rapid acid generating capacity of the fertiliser. The low pH of the column E and F coating stage leachates does not appear to have affected phosphate development within the columns, which is in contradiction to the observations Evangelou (1995b) made on pyrite. The low pH of column G may have been responsible for the less abundant phosphate development observed in that column, however, it is possible that the lack of a strong oxidant was a more important factor.

Stability of phosphate phases

The abundant phosphate coatings observed in columns A, B, E and F inhibited acid generation more effectively then the coatings developed in experiments 1 and 2. The thin and heterogeneous Fe-K-Cu phosphate coatings observed in column C material were not as effective in preventing acid generation (Fig.

3.17a). This indicates that an oxidant is required to form the most effective phosphate coatings. The continued rise in pH of the column F and G leachates was probably caused by decreasing dissolution of relict Trifos, small (200 μm diameter), partly dissolved particles of which were observed on the waste material removed from columns E, F and G after the dissolution stage. The column G leachate stabilised at a lower pH than columns E and F (Fig. 3.17a). This indicates the phosphate coatings formed in column G, without an aggressive oxidant in the coating solution and at lower pH during the coating stage, were not as effective at inhibiting acid generation.

The base metal concentrations of the column A – F leachates during the dissolution stage were all one to two orders of magnitude less than the control column leachate values (Fig. 3.18c,e,f). This was due to the reduced metal release from inhibited sulphide oxidation and the low mobility of the metal cations at the higher pH values of the column A – F leachates. The removal of substantial amounts of the metal-bearing granular Mn/Ca phosphates from the coated columns during the dissolution stage probably had little effect on the dissolved metal leachate concentrations. The observation of flushing of significant amounts of precipitate out of the columns during the dissolution stage implies that the granular Mn/Ca phosphates were only partially disassociated. It is therefore likely that the metals incorporated into the granular Mn/Ca phosphates remained in colloidal or larger particles rather than being released as dissolved cations into the leachate. The higher base metal and Fe concentrations in the column G leachates during the dissolution stage (Fig. 3.18c,e,f,h) were probably due to higher mobility of dissolved metal cations at the lower pH of the leachate. The metal cations were probably sourced from sulphide oxidation and disassociation of metal cations from the granular Ca phosphate precipitates. The phosphate coatings and granular precipitates observed in column G were less effective at sulphide oxidation inhibition and metal attenuation than the phosphates observed in columns A, B, E and F.

The concentration trends of Sb in the dissolution stage leachates, except for column C, differed markedly from experiment 1 and 2, and also from the trends

of [As] (Fig. 3.18a,g). The low [Sb] at the start of the dissolution stage in columns A, B, E, F and G was probably partly due to the relatively low mobility of Sb in the slightly acidic pH of the dissolution stage leachates compared with the other experiments. However, leachate pH cannot account for all of the observed Sb trends. Column E and F leachates (pH 6–7) had [Sb] only slightly greater than the control column leachates (pH 4.2), whereas the column G leachates (pH ~5.5) had higher [Sb] than column E and F. Phosphate coatings were observed on tetrahedrite in all columns except column C, most abundantly in columns E and F (Fig. 3.16b; Fig. 3.19c). These coatings probably inhibited tetrahedrite oxidation and prevented subsequent Sb release, particularly in columns E and F.

The high [SO_4^{2-}] in the coated column leachates was again problematic (Fig. 3.18b). It was expected that control column leachate [SO_4^{2-}] would have been higher than the coated column values due to greater sulphide oxidation. Desorption/disassociation of SO_4^{2-} from the Mn and Ca phosphate precipitates, particularly in columns A and B, may be partly responsible for the high [SO_4^{2-}] in the leachates of the coated columns during the dissolution stage. The processes controlling the [SO_4^{2-}] in the leachates are not well understood and further work is required to ascertain why [SO_4^{2-}] in the control column leachates are not well above the coated column values.

3.5.6 Summary

The use of $KMnO_4$ as an oxidant and the fertilisers MKP and Trifos as sources of phosphate provided abundant cations for the formation of phosphate coatings and precipitates. These phosphates proved to be very efficient at inhibiting sulphide oxidation and attenuating metal release in the column leaching experiments. The presence of an oxidant was still necessary for the formation of abundant phosphate coatings which inhibited sulphide oxidation. All sulphides, including tetrahedrite, were coated to some degree, although chalcopyrite and galena were still the most abundantly coated sulphides.

Acid generation was inhibited throughout the dissolution stage in columns A, B, E and F. The column C leachate pH decreased steadily during the dissolution stage probably because the heterogeneous, poorly-formed phosphate coatings observed in the column only partially inhibited sulphide oxidation. The continual rise in pH of column G leachates was probably due to decreasing dissolution of relict Trifos particles within the columns.

Dissolution stage metal release was inhibited in all columns relative to the control column. Column G leachate metal concentrations were significantly higher than the other coated column leachates. The dissolution stage concentrations of Sb were lower than in experiments 1 and 2 with the exception of column C. This was probably due to the development of coatings on tetrahedrite, which were not observed in experiments 1 and 2.

3.6 Experimental limitations

Several limitations of the experimental methodology became apparent during operation and interpretation of the experiments. These limitations are related to the column experiments themselves or to the analytical methods used to characterise the waste material and phosphate phases formed in the coated columns.

3.6.1 Phosphate stabilisation experiments

The control columns in the phosphate stabilisation experiments did not undergo an identical process to the coated columns. The application of the coating solution to the coated columns most likely dissolved any soluble sulphates present in the waste. Thus, at the start of the dissolution stage, the soluble sulphates present in the control column would dissolve with the first application of the oxidising solution, whereas in the coated columns the sulphates had already been removed. This would have caused the dissolved elemental concentrations in the control column leachates to be anomalously high compared with the coated column leachates. The validity of the experiments is

not compromised by this limitation because with continued leaching during the dissolution stage, the elemental concentrations in the control column leachates were controlled mainly by sulphide oxidation.

$Ca(OH)_2$ was not added to the control columns in order to determine the ability of the phosphate coating to inhibit acid generation. The resulting low pH of the control columns raises the possibility that the base metal concentrations in the dissolution stage leachates were controlled by the leachate pH alone and not by phosphate attenuation. SEM observations support the control of base metal values by phosphate attenuation, particularly the corroded phosphate phases observed in experiment 2. However, further experimentation should include a control column to which $Ca(OH)_2$ is added to investigate whether metal attenuation occurs to the same degree at circum-neutral pH without the presence of phosphate.

The presence of precipitates was observed in many of the column leachates, particularly at the beginning of the experimental stages. Samples were decanted before analysis in an attempt to remove all precipitates from the sample solution. However, it is possible that some precipitates may have been in the analysed sample, particularly in experiment 3, in which extensive precipitates were observed in some samples (Section 3.5.4). The presence of precipitates in the analysed sample would be of concern as the precipitates may contain significant adsorbed metals (Section 3.5.5). This may be an explanation for the slightly anomalous base metal values in several of the dissolution stage leachates in experiment 3 (Fig. 3.18) (Y. Hu, pers. comm. 2003). Future experiments should filter the leachate samples through 0.45 μm filter paper to ensure that there are no precipitates present in the samples. This would also allow collection and analysis of the precipitates, extending knowledge of the speciation and mobility of elements in colloidal phases in the phosphate stabilisation experiments.

Only one set of columns were used for each experiment. In similar column leaching experiments Vandiviere and Evangelou (1998) used replicate columns

and discovered large variations in results between replicates. The use of replicate columns in further experiments would ensure a more scientifically rigourous methodology.

3.6.2 Waste characterisation

The use of XRD to characterise waste mineralogy has some inherent limitations, particularly complex material such as that used in the phosphate stabilisation experiments. The detection limit of XRD is relatively low, ~1 wt.% (Ma et al., 1994). The presence of <1 % of a highly soluble mineral such as melanterite or chalcanthite on grain surfaces of waste material may have a significant effect on leachate chemistry. However, at this abundance, the mineral would not be detected by XRD. Furthermore, minerals with a well defined cleavage pattern, such as clays, micas and anglesite (Ruby et al., 1994) may lie in a preferred orientation in the powder mount. This can create a trace with exaggerated peaks of some minerals and with understated peaks of other minerals. Therefore, the exact mineralogy of the waste used in the columns is not known, particularly those minerals present in trace amounts. This has created some uncertainty regarding the nature of the hosts of some elements in the waste material. However, the major phases controlling the chemistry of the column leachates were generally well understood and few assumptions needed to be made.

3.6.3 Scanning electron microscopy

The majority of SEM observations of coated column material were made using carbon-coated stubs. The carbon coating allows surface chemistry to be analysed by EDS. However, image clarity at magnifications >5000x is poor. Therefore, very fine details such as the granular precipitates on chalcopyrite shown in Figure 3.7b were not observed until the grains were gold-coated, which precludes surficial EDS analysis. Thus, it was impossible to determine the chemistry of many very fine-grained phases observed in the material removed from the columns.

The depth of penetration of the SEM-EDS is generally 1-3 μm (K. Blake, pers. comm. 2003). Therefore, analysis of very thin coatings will also detect elements within the substrate. This makes determination of the exact chemistry of thin phosphate coatings very difficult or impossible. The determination of the exact chemistry of thin phosphate coatings and fine-grained precipitates observed in the coated columns requires more delicate surficial analytical techniques.

Only 10-20 grains were collected for SEM observations from each column at the conclusion of the coating and dissolution stages of each experiment. This was only a very small fraction (<0.5 %) of the total waste present in the columns. Although the grains were selected from all parts of the columns, it is possible that the samples observed were not representative of all of the column material. The observed heterogeneity of some phases, particularly the Cu phosphate rosettes, indicates that phosphate development varied within the columns. Observations of the more common phases in the columns (e.g. Fe-K phosphates, Pb phosphates and Mn or Ca phosphates) were probably not affected by the small sample size. However, the apparent paucity of some phases, such as the Zn phosphates in Columns A and B of experiment 1, may be a result of the small sample size and heterogeneous phosphate development.

3.7 Summary of phosphate stabilisation experiments

The experiments demonstrate that phosphate coatings and precipitates can be induced in:

- polyminerallic, sulphidic mine waste and
- partly oxidised, polyminerallic mine waste

using....

- liquid phosphate stabilisers,
- liquid phosphate fertilisers, and
- solid phosphate fertilisers.

The coatings were created by leaching the material with a solution of KH_2PO_4, H_2O_2 and CH_3COONa (experiments 1 and 2) or CH_3COONa, liquid or solid fertiliser $\pm$ $KMnO_4$ (experiment 3). Dissolution stage leachate analyses indicate that coated mine wastes release significantly less acid and dissolved base metals than the uncoated waste due to reduced sulphide oxidation and immobilisation of metals into phosphate phases.

Metal $\pm$ alkali phosphate coatings developed to some degree on all sulphide minerals present in the waste of experiment 3 and on all sulphide minerals except tetrahedrite in the waste of experiments 1 and 2. Pyrite was only occasionally and poorly coated in experiments 1 and 2. In all experiments, the strength of the oxidant was the most important factor controlling phosphate development. In partly oxidised waste, the dissolution of secondary minerals provided abundant metal cations, which reacted with the phosphate anions to form solid phosphate phases. Such phase formation inhibited acid generation in all columns. In experiment 3, the fertilisers MKP and Trifos, and the use of $KMnO_4$ as an oxidant provided abundant cations to complex with the phosphate, resulting in extensive Mn and Ca phosphates that often contained major amounts of metals.

The long-term ability of the phosphates to reduce dissolved metal concentrations in the leachate was dependent on the stability of the phases in the oxidising solution. Fe-K and Pb phosphates were very stable during the dissolution stage of experiments 1 and 2, preventing the release of Fe and Pb into the leachates. The Zn and Cu concentrations increased throughout the dissolution stage of experiments 1 and 2 due to gradual corrosion of the Cu-Ca and Zn-K phosphates. Dissolved metal leachate concentrations were reduced throughout the dissolution stage of experiment 3 due to the stability of the amorphous Mn phosphates which retained their incorporated metals. The concentrations of As and Sb in the leachate were higher in the coated columns of all experiments due to greater mobility of these metalloids at elevated pH values.